CHIN. PHYS. LETT. Vol. 29, No. 5 (2012) 057201

Exact Results for Intrinsic Electronic Transport in Graphene *

HU Shi-Jie(胡时杰)[1,2†], DU Wei(杜巍)[1†], ZHANG Gui-Ping(张桂平)[1], GAO Miao(高淼)[1], LU Zhong-Yi(卢仲毅)[1], WANG Xiao-Qun(王孝群)[1**]

[1]*Department of Physics, Renmin University of China, Beijing 100872*
[2]*Institute of Theoretical Physics, Chinese Academy of Sciences, Beijing 100190*

(Received 14 March 2012)

We present exact results for the electronic transport properties of graphene sheets connected to two metallic electrodes. Our results obtained by transfer-matrix methods are valid for all sheet widths and lengths. In the limit of the large width-to-length ratio relevant to recent experiments, we find a Dirac-point conductivity of $2e^2/\sqrt{3}h$ *and a sub-Poissonian Fano factor of* $2-3\sqrt{3}/\pi \simeq 0.346$ *for armchair graphene; for the zigzag geometry they are respectively 0 and 1. Our results reflect essential effects from both the topology of graphene and the electronic structure of the leads, giving a complete microscopic understanding of the unique intrinsic transport in graphene.*

PACS: 72.80.Vp, 73.22.Pr, 74.25.F−, 73.40.Sx DOI: 10.1088/0256-307X/29/5/057201

Graphene, a graphite monolayer of carbon atoms forming a honeycomb lattice, has a distinctive electronic structure whose low energy excitations are described by massless Dirac fermions. The successful extraction of micron-scale graphene sheets from a natural graphite crystal, as well as their deposition onto an oxidized Si wafer,[1] was a truly seminal event which ushered in a new era of realistic experimental and theoretical exploration. The subsequent explosion of graphene activity has focused on fundamental questions concerning the transport properties of relativistic particles in graphene and on its potential applications as a high-mobility semiconductor.

Theoretical predictions[2] for two-dimensional Dirac-fermion systems give an intrinsic conductivity σ_0 of order e^2/h. Minimal conductivities around this value were observed at the Dirac point[3] in Ref. [1] while later measurements[4] suggested that $\sigma_0 \to 4e^2/\pi h$ when the width-to-length ratio of the sample is sufficiently large. This is the value obtained by using massless Dirac fermions and graphite leads in a Landauer-Büttiker (LB) formulation.[5,6] It is associated with a maximum of 1/3 in the Fano factor F_0,[6] which reflects the partial transmission of quantized charge through the finite graphene system. Measurements of the current shot noise in both ballistic[7] and diffusive[8] graphene systems have indeed found that $F_0 \approx 1/3$ in short and wide samples. Many authors have addressed different aspects of the graphene transport problem, as summarized in the following. While the finite conductivity and suppressed Fano factor are generally expected in graphene systems, the underlying physics remains rather poorly understood, not least because the carrier density at the Dirac point is zero.

In this Letter, we consider graphene sheets of both armchair (AGS) and zigzag (ZGS) geometries, connected to two metallic leads as illustrated in Fig. 1. By establishing a transfer-matrix formulation within this minimal model, we present exact results for the anomalous intrinsic transport properties of graphene. We demonstrate that the AGS and ZGS are completely different, and explain in detail the non-universal dependences of σ and F on geometry, filling, and gate voltage.

The low-energy properties of graphene can be described by a nearest-neighbor one-orbital tight-binding model for π-electrons on a hexagonal lattice,

$$H = -t_2 \sum_{\langle ij,i'j'\rangle} c_{ij}^{\dagger} c_{i'j'} + \mu \sum_{ij} c_{ij}^{\dagger} c_{ij}, \qquad (1)$$

where $c_{ij}^{\dagger}$ is an electron creation operator at lattice site $\boldsymbol{r}_{ij} \equiv (x_i, y_j)$, $\langle\cdot\rangle$ denotes the nearest-neighboring sites, t_2 is the hopping integral, and μ the chemical potential. The two electrodes are represented by semi-infinite rectangular strips with hopping t_0, while the interface hopping is t_1. We take the interface contact to be perfect and impose open boundary conditions on the two free edges of the sheet; it is the geometry of these edges which determines our nomenclature (AGS or ZGS). Because graphene has two sublattices, sheets are taken to have $N = 4m$ (AGS) or $M = 4m$ (ZGS) with m being an integer.

We begin with the AGS case (Fig. 1) by constructing a transfer-matrix equation for the scattering of electrons between two electrodes. In the Schrödinger equation $\hat{H}\psi(E) = E\psi(E)$, the wave function is represented as $\psi(E) = \sum_{ij} \alpha_{ij}|ij\rangle$ [$|ij\rangle = c_{ij}^{\dagger}|0\rangle$ for $\boldsymbol{r}_{ij}$], with the complex coefficients α_{ij} to be determined. $E = E_{\rm F}$ is the Fermi energy of the electrodes, which is set by their occupation n_c. There are M right-traveling and M left-traveling waves (channels) in each electrode, each channel characterized by a trans-

*Supported by the Research Foundation from Ministry of Education of China (2009EDU309002), the National Basic Research Program of China (2012CB921704), and the National Natural Science Foundation of China under Grant No 11174363.
**Correspondence author. Email: xiaoqunwang62@gmail.com
†Contributed equally to this work.
© 2012 Chinese Physical Society and IOP Publishing Ltd

verse wavenumber $k_y^n = \frac{n\pi}{M+1/2}$ with $n = 1, \ldots, M$. The longitudinal wavenumber k_x^n is related to k_y^n by $E_{\rm F} = -2t_0(\cos k_x^n + \cos k_y^n)$.

With a unit-amplitude right-traveling wave incident on the sheet in the nth channel of the left electrode, for the left and right electrodes we have

$$\alpha_{ij}^L = \sum_{n'} (\delta_{n'n} e^{ik_x^{n'} x_i} + r_{n'n} e^{-ik_x^{n'} x_i}) \sin(k_y^{n'} y_j),$$
$$\alpha_{ij}^R = \sum_{n'} t_{n'n} e^{ik_x^{n'} x_i} \sin(k_y^{n'} y_j), \qquad (2)$$

where $r_{n'n}$ and $t_{n'n}$ are respectively reflection and transmission coefficients from channel n to n'. For each site $\boldsymbol{r}_{ij}$ in the sheet, $\sum_{\tau,\delta} \alpha_{i+\tau,j+\delta} = \tilde{\mu}\alpha_{ij}$, where τ and δ specify the nearest-neighboring sites of $\boldsymbol{r}_{ij}$ and $\tilde{\mu} = (\mu - E_{\rm F})/t_2$. We express the M coefficients α for a given i as the vector $\boldsymbol{\alpha}_i = (\alpha_{i1}, \ldots, \alpha_{iM})^T$ in order to connect $\boldsymbol{\alpha}_i$ with its neighboring slices through the $2M \times 2M$ transfer matrix $\mathcal{T}_i$,

$$\begin{bmatrix} \vec{\alpha}_{i-1} \\ \vec{\alpha}_i \end{bmatrix} = \mathcal{T}_i \begin{bmatrix} \vec{\alpha}_i \\ \vec{\alpha}_{i+1} \end{bmatrix} \qquad (3)$$

A translation period involves four different slices (Fig. 1), so $\mathcal{T}_i$ cycles through the four 2×2 block matrices

$$A = \begin{bmatrix} \tilde{\mu}I & -X^T \\ I & 0 \end{bmatrix}, \quad B = \begin{bmatrix} \tilde{\mu}Y & -Y \\ I & 0 \end{bmatrix},$$
$$C = \begin{bmatrix} \tilde{\mu}I & -X \\ I & 0 \end{bmatrix}, \quad D = \begin{bmatrix} \tilde{\mu}Y^T & -Y^T \\ I & 0 \end{bmatrix}, \qquad (4)$$

where X is lower-bidiagonal with nonzero elements equal to 1, Y is the inverse of X, and I is the identity.

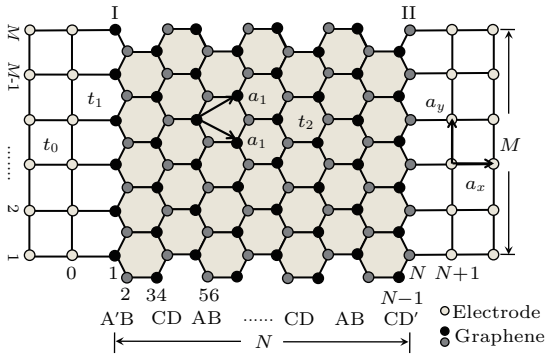

Fig. 1. Schematic representation of an armchair graphene sheet connected to electrodes at interfaces I and II. Primitive vectors $\boldsymbol{a}_x$ and $\boldsymbol{a}_y$ for the electrodes and $\boldsymbol{a}_1$ and $\boldsymbol{a}_2$ for the sheet give length $L = \sqrt{3}N|\boldsymbol{a}_1|/4$ and width $W = (M-1)|\boldsymbol{a}_1|$, with $N \times M$ sites; $a_1 = a_2 = a_y$ with $a_1 = 2.46$ Å for graphene. The ZGS case, obtained by a $\pi/2$ rotation, has length $L = N|\boldsymbol{a}_1|$ and width $W = \sqrt{3}M|\boldsymbol{a}_1|/4$, with $(N+1/2) \times M$ sites.

Recursive application of Eq. (3) for N slices ($N/4$ translation periods) relates the coefficients α^L and α^R at the left and right interfaces through

$$\begin{bmatrix} \boldsymbol{\alpha}_0^L \\ \boldsymbol{\alpha}_1^L \end{bmatrix} = \begin{bmatrix} \tilde{t}_2 I & 0 \\ 0 & I \end{bmatrix} (ABCD)^{\frac{N}{4}} \begin{bmatrix} I & 0 \\ 0 & \tilde{t}_1 I \end{bmatrix} \begin{bmatrix} \boldsymbol{\alpha}_N^R \\ \boldsymbol{\alpha}_{N+1}^R \end{bmatrix}, \qquad (5)$$

where $\tilde{t}_1 = t_1^2/(t_0 t_2)$, $\tilde{t}_2 = 1/\tilde{t}_1$. By considering the one-period transfer matrix $ABCD$, one finds that the transverse modes in the AGS are unmixed by scattering processes, remaining independent and retaining the free-particle dispersion $\epsilon_n = -2 - 2\cos k_y^n$. This makes the LB formalism underlying our transport calculations particularly appropriate. Thus Eq. (5) can be decomposed into a set of binary linear equations,

$$\begin{bmatrix} -\tilde{t}_1 & g_n \\ -e^{-ik_x^n} & h_n \end{bmatrix} \begin{bmatrix} r_{nn} \\ t_{nn} \end{bmatrix} = \begin{bmatrix} \tilde{t}_1 \\ e^{ik_x^n} \end{bmatrix},$$
$$\begin{bmatrix} g_n \\ h_n \end{bmatrix} = \begin{bmatrix} a_n & b_n \\ -b_n & c_n \end{bmatrix}^{\frac{N}{4}} \begin{bmatrix} 1 \\ \tilde{t}_1 e^{ik_x^n} \end{bmatrix}, \qquad (6)$$

with $a_n = (\tilde{\mu}^2 - \tilde{\mu}^4)\epsilon_n^{-1} - 2\tilde{\mu}^2 - \epsilon_n$, $b_n = (\tilde{\mu}^3 - \tilde{\mu})\epsilon_n^{-1} + \tilde{\mu}$, $c_n = (\tilde{\mu}^2 - 1)\epsilon_n^{-1}$, and $a_n c_n + b_n^2 = 1$.

Analytic solution for t_{nn} from Eq. (6) gives the transmission probability $T_n \equiv T(k_y^n) = |t_{nn}|^2$ as

$$T_n = \frac{1}{\gamma_1 \cosh(N\theta_n/2) + \gamma_2 \sinh(N\theta_n/2) + \gamma_3}, \qquad (7)$$

where $\gamma_1 = (\nu_1^2 + \nu_2^2 + \nu_3^2 + \nu_4^2)/8$, $\gamma_2 = \mathrm{sign}(\kappa_\pm^2)(\nu_1\nu_2 + \nu_3\nu_4)/4$, $\gamma_3 = (-\nu_1^2 + \nu_2^2 - \nu_3^2 + \nu_4^2)/8$, $\nu_1 = (-2\xi_- + \xi_+\tilde{t}_+ \cos k_x^n)/\sin k_x^n$, $\nu_2 = \tilde{t}_- \cos k_x^n / \sin k_x^n$, $\nu_3 = \xi_+\tilde{t}_-$, $\nu_4 = \tilde{t}_+$, $\xi_\pm = (\kappa_+/\kappa_- \pm \kappa_-/\kappa_+)/2$, $\kappa_\pm = (c_n - a_n \pm 2b_n)^{1/2}$, $\tilde{t}_\pm = \tilde{t}_1 \pm \tilde{t}_2$, and $\cosh\theta_n = (a_n + c_n)/2$. The conductivity σ and Fano factor F may now be computed exactly from Eqs. (6) and (7), leading to

$$\sigma = \frac{\sqrt{3}N}{4M} \frac{2e^2}{h} \sum_n T_n, \qquad F = \frac{\sum_n T_n(1 - T_n)}{\sum_n T_n}. \qquad (8)$$

These expressions are completely general within the LB framework, and are applicable for all sheet sizes (N, M).

For present purposes, we focus on the physical insight contained in Eq. (8) for the situation relevant to most graphene experiments, namely wide electrodes patterned onto the sample with rather narrow separation.[7,8] In this limit of large $W/L(\sim M/N)$, the sum in Eq. (8) is replaced by an integral over k_y. For convenience we set $t_0 = t_1 = t_2$, which creates no special symmetries. The Dirac-point conductivity σ_0 and the corresponding Fano factor F_0 may then be expressed analytically as

$$\sigma_0 = \frac{e^2}{h} \frac{2\sqrt{3}\arctan(|\cos k_x^c / \sin k_x^c|)}{\pi \sin k_y^c |\cos k_x^c / \sin k_x^c|},$$
$$F_0 = \frac{1}{2}\sec^2 k_x^c - \frac{|\sin k_x^c / \cos k_x^c|}{2\arctan(|\cos k_x^c / \sin k_x^c|)}, \qquad (9)$$

where k_y^c is the Dirac-point wavenumber $2\pi/3$ of the AGS and k_x^c is determined by $E_{\rm F}$. At half-filling of the electrodes, *i.e.* $n_c = 1$ and $E_{\rm F} = 0$, we obtain $\sigma_0 = 2e^2/\sqrt{3}h \approx 1.1547e^2/h$ and $F_0 = 2 - 3\sqrt{3}/\pi \approx 0.3460$.

Our results for the AGS are similar but not identical to the values $4e^2/\pi h$ and 1/3 of Ref. [6]. While the electronic structure of the electrodes leads to a small

quantitative difference between the two studies, we will show in the following that the symmetry-breaking effect of the electrode interfaces causes a strong qualitative difference. The fact that $\sigma_0 \neq 0$ at the Dirac point $\tilde{\mu} = 0$, despite the vanishing density of states, is an intrinsic property of the AGS quite distinct from conventional mesoscopic systems.

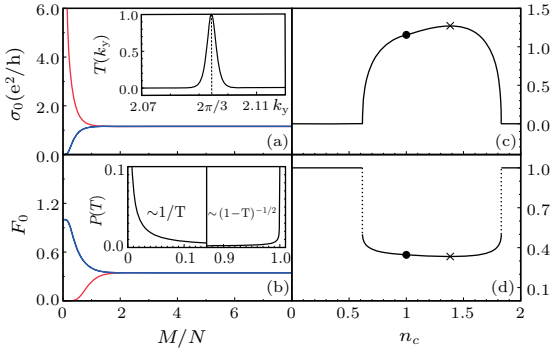

Fig. 2. (Color online) Dirac-point conductivity σ_0 (a,c) and Fano factor F_0 (b,d) versus M/N for $n_c = 1$ (a,b) and versus n_c with $M/N = 10$ (c,d). Dots denote $\sigma_0 = 2e^2/\sqrt{3}h$ in (c) and $F_0 = 2-3\sqrt{3}/\pi$ in (d) at $n_c = 1$, while crosses denote $\sigma_0 = 4e^2/\pi h$ in (c) and $F_0 = 1/3$ in (d), obtained at $n_c \approx 1.39$. Insets: transmission probability $T(k_y)$ around $k_y^c = 2\pi/3$ in (a) and its distribution $P(T)$ (see text) in (b). Calculations performed with $N = 1000$ in the system shown in Fig. 1.

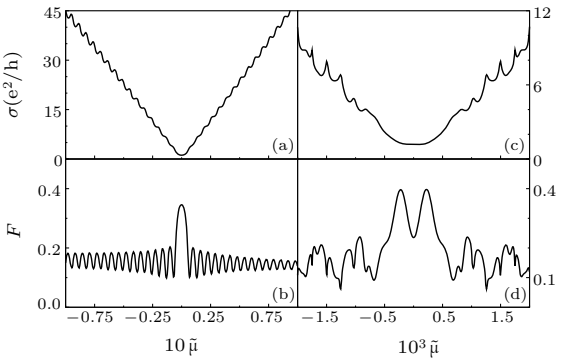

Fig. 3. Conductivity σ (a,c) and Fano factor F (b,d) for the AGS with $M = 10000$ and $n_c = 1$, versus $\tilde{\mu}$ for $M/N = 10$ (a,b) and $M/N = 1$ (c,d).

To analyze the physical origin of this behavior, Fig. 2 shows the full dependence of σ_0 and F_0 on n_c and on the aspect ratio M/N of the sheet for $\tilde{\mu} = 0$. In Figs. 2(a) and 2(b), for $n_c = 1$, σ_0 and F_0 alternate as M increases between semiconducting and metallic behavior, the latter obtained when $\mathrm{mod}(2M+1, 3) = 0$ and there exists a resonant channel with $T_n = 1$ at $k_y^n = k_y^c$ [inset in Fig. 2(a)]. As the sheet width is increased, the two branches merge at $M/N \sim 1.5$ with σ_0 and F_0 independent of M/N, only when $M \gtrsim N$ are sufficiently many channels with $T_n \sim 1$ available that their contributions to the sum in Eq. (8) are constant. For such sheets [inset in Fig. 2(b)], channels with $T \gtrsim 0.9$ contribute to F_0 with a distribution $P(T) \propto 1/\sqrt{1-T}$ while channels with $T \lesssim 0.1$ have $P(T) \propto 1/T$.[9] Although $P(T)$ resembles the universal bimodal distribution for a disordered mesoscopic system, which also has $F_0 \sim 1/3$, the underlying physics is completely different: the sub-Poissonian behavior is caused by the interference of relativistic quantum particles, which results in transport contributions $T_n \sim \exp(-|k_y^n - k_y^c|N)$ away from the resonant channel [inset in Fig. 2(a)]. This type of behavior, namely $\sigma_0 \neq 0$ and $F_0 \sim 1/3$, is obtained in the AGS only for $0.63 \lesssim n_c \lesssim 1.83$ [Figs. 2(c) and 2(d)].

Figure 3 shows the effects of a gate voltage on σ and F for $n_c = 1$. For a finite sheet, the number of Fermi momenta (number of energy bands intersected) increases with μ, and each peak in σ and F corresponds to one more contributing resonant channel. When the sheet is sufficiently wide [Fig. 3(a)], channels are added at nearly equal intervals, resulting in almost periodic oscillations, whereas for $M/N \lesssim 1.5$ [Fig. 3(b)] the effects of added channels appear to be quasi-periodic, superposed on that the oscillation is a linear and slightly asymmetric behavior of σ about the Dirac point. The former is a consequence of the linear dispersion of graphene and the latter of the electron-hole asymmetry caused by the electrodes.[10] Thus our exact results illustrate the inherent dependence of experimental observations on both W/L and L,[3,4] and demonstrate further that such behavior can be intrinsic, rather than appearing only as a consequence of sample disorder or interfacial defects.

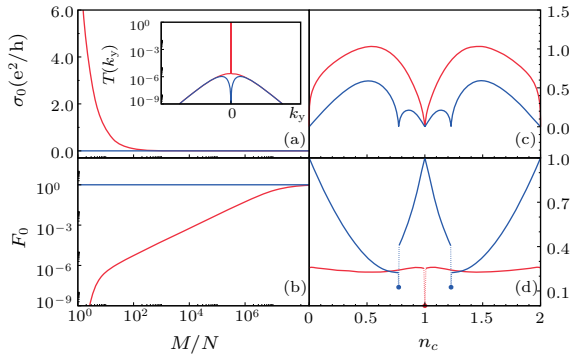

Fig. 4. (Color online) σ_0 (a,c) and F_0 (b,d) for a ZGS, versus M/N at $n_c = 1$ (a,b) and n_c for $M/N = 1200$ (c,d). Inset: $T(k_y)$ around $k_y^c = 0$. Red and blue curves indicate respectively metallic and semiconducting situations, calculated with $N = 1000$ and 999.

Now we turn to the ZGS. The geometry of this case requires a transfer matrix $\mathcal{T}_i$ expressed in terms of two 2×2 block matrices and a quartic form of Eq. (6) for t_{nn}, which is solved numerically to obtain σ and F from Eq. (8). Figure 4 shows the dependences of σ_0 and F_0 on M/N, again with $t_0 = t_1 = t_2$ and $\tilde{\mu} = 0$. The ZGS also possesses metallic and semiconducting branches, which alternate with respect to the sheet length N rather than to its width M. The asymptotic behavior is metallic, with $\sigma_0^u \propto 16/\sqrt{3}\frac{M}{N}$ for $\mathrm{mod}(2N+1, 3) = 0$, and semiconducting with $\sigma_0^d \sim 0.2801/N^2$ otherwise [Fig. 4(a)]. The corresponding Fano factors [Fig. 4(b)] are $F_0^u \sim (1 - 0.2801/N^2)/(1 + 32.98N^2/\frac{M}{N})$ and $F_0^d \sim 1 - 0.08223/N^2$, the two branches merging only

when $\frac{M}{N} \gg 32.98N^2$. Graphene sheets in this limit of W/L would therefore have $\sigma_0 = 0$ and $F_0 = 1$ at the Dirac point, implying a Poissonian shot-noise quite different from the AGS. A finite minimal conductivity, $\sigma_0 \lesssim 2e^2/\sqrt{3}h$ (reaching its maximal value when $E_F = \pm 1$), and a sub-Poissonian F_0 are obtained for all $n_c \neq 0, 1, 2$ [Figs. 4(c) and 4(d)].

The origin of the contrasting intrinsic transport properties of the AGS and ZGS for the Dirac point lies in the special nature of zigzag chains in graphene. The key point is how this affects scattering at the interfaces. Because $\sum_{\tau,\delta} \alpha_{i+\tau,j+\delta} = 0$ for any site $\boldsymbol{r}_{ij}$ in the sheet, the wavenumber of extended states is $2\pi/3$ when projected onto the zigzag chain direction, and zero in the orthogonal direction. In the AGS, zigzag chains are parallel to the interfaces so that $k_y^c = 2\pi/3$ for $\mathrm{mod}(2M+1, 3) = 0$. Thus the incident traveling wave is not deformed at the interface and there is no interfacial scattering. Consequently, $T(k_y^c) = 1$ and $T(k_y^n) \sim 1$ in a regime of width $O(1/L)$ about k_y^c [inset in Fig. 2(a)], resulting in a finite σ_0 after the summation in Eq. (8) if $0.63 \lesssim n_c \lesssim 1.83$ [Fig. 2(c)]. In the ZGS, zigzag chains connect the left and right electrodes, $k_y^c = 0$, and the armchair interfaces involve two sublattices, with two values of k_x^n corresponding to each k_y^n. This induces interfacial scattering. As a consequence, for $n_c = 1$ the transmission amplitudes are suppressed very strongly for any $k_y^n \neq k_y^c$ and $T_n = \delta_{k_y^n, k_y^c} + T_b$ [inset in Fig. 4(a)], where T_b is a very small background of width $O(1/L^3)$ arising from interfacial scattering. Neither term contributes to the integral in the limit of large W/L and L, whence $\sigma_0 = 0$ and $F_0 = 1$. When $n_c \neq 1$,[18] imaginary k_x^n values appear for some channels $\{k_y^n\}$, giving contributions to $T(k_y^n)$ over a greater width and leading to a finite σ_0 [Fig. 4(c)]. Thus it is the topological difference in the geometry along and across a hexagonal lattice which results in two fundamentally different types of interfacial scattering, and hence in the contrasting intrinsic transport properties of AGS and ZGS systems. This microscopic insight was not included in any previous study.

Many investigations of graphene transport may be found in recent literature. Augmenting the general results cited above, experimental studies of the conductivity minimum have addressed the coherence of Dirac-point transport,[11] the role of contacts and sample edges,[12] and how interface charging leads to asymmetric gate-voltage effects.[13] Many theoretical studies have considered transmission coefficients in a finite graphene system, all restricted (as here) to the case of non-interacting electrons: from its weak interactions and the vanishing density of states at the Dirac point, the fundamental transport properties of graphene are expected to emerge at the band-structure level. These investigations all differ from ours in the approximations applied, or in system size and geometry, or in the method of calculation, and hence in the nature of their conclusions. In an effective contact model[14] for a sufficiently large system, mode selection at the Dirac point makes all leads equivalent. Numerical treatments, of the same model[15] and in a more general framework,[16] have probed size, gate-voltage, and impurity effects. While these and other studies[6,17] note that the AGS and ZGS cases should differ from each other, the fundamentally different nature ($\sigma_0 = 0$, $F_0 = 1$) of the ZGS case and the microscopic origin of the different intrinsic transport properties have been missed. Further, because we have analyzed the intrinsic transport arising due to lead and interface geometry, we may conclude that disorder effects are not required to obtain the anomalous behavior observed in experiment.[3,4,11]

In summary, we have presented exact solutions of the transfer-matrix equations for graphene sheets with metallic electrodes. Our results are microscopic and completely general, and can be used to show that the Dirac-point conductivity and the Fano factor tend respectively to $\sigma_0 = 2e^2/\sqrt{3}h$ and $F_0 = 2 - 3\sqrt{3}/\pi$ for armchair graphene sheets in the short and wide limit relevant to experiments. The same quantities tend to 0 and 1 respectively for zigzag graphene sheets. Our exact results suggest that the measured finite minimum conductivity and sub-Poissonian Fano factor are the consequence of armchair rather than zigzag graphene systems, and show how this fundamental difference depends on the availability of resonant transmission channels, which is determined in turn by the geometry of the hexagonal lattice.

The authors thank B. Normand, E. Tosatti, B. G. Wang, X. R. Wang, X. C. Xie, Lu Yu, and Y. S. Zheng for fruitful discussions.

References

[1] Novoselov K S et al 2004 *Science* **306** 666
[2] Fradkin E, 1986 *Phys. Rev.* B **33** 3263
Shon N H and Ando T 1998 *J. Phys. Soc. Jpn.* **67** 2421
Gorbar E V, Gusynin V P, Miransky V A and Shovkovy I A 2002 *Phys. Rev.* B **66** 045108
[3] Novoselov K S et al 2005 *Nature* **438** 197
[4] Miao F et al 2007 *Science* **317** 1530
[5] Katsnelon M I, 2006 *Eur. Phys. J.* B **51** 157
[6] Tworzydło J et al 2006 *Phys. Rev. Lett.* **96** 246802
[7] Danneau R et al 2008 *Phys. Rev. Lett.* **100** 196802
[8] DiCarlo L et al 2008 *Phys. Rev. Lett.* **100** 056801
[9] The distribution of the transmission probability is defined as $P(T) = \frac{1}{\pi}\partial k_y/\partial T$
[10] When graphite leads are used, σ is symmetric.[6]
[11] Heersche H B et al 2007 *Nature* **446** 56
[12] Lee E J H et al 2008 *Nature Nanotech.* **3** 486
[13] Huard B, Stander N, Sulpizio J A and Goldhaber-Gordon D 2008 *Phys. Rev.* B **78** 121402
[14] Schomerus H, 2007 *Phys. Rev.* B **76** 045433
[15] Robinson J P and Schomerus H 2007 *Phys. Rev.* B **76** 115430
[16] Barraza-Lopez S, Vanević M, Kindermann M and Chou M Y 2010 *Phys. Rev. Lett.* **104** 076807
[17] Blanter Y M and Martin I 2007 *Phys. Rev.* B **76** 155433
[18] Detailed analysis for $n_c \neq 1$ will be presented elsewhere